Research Article GU J Sci 37(2): 774-791 (2024) DOI: 10.35378/gujs.1232730

Gazi University

Journal of Science

http://dergipark.gov.tr/gujs

Reflective Polarization Conversion with Multi-Functional, Ultrathin Metasurface for Ku- and K-Band Applications

Ahmet TEBER*

Bayburt University, Department of electrical and Energy, 69000, Bayburt, Türkiye

Highlights

- This paper represents an ultrathin, single-layered, and multi-functional polarization converter.
- The substrate thickness has a multi-functional effect on polarization conversion.
- Good performances and multi-functional properties were obtained for Ku- and K-band applications.

Article Info

Received: 11 Jan 2023
Accepted: 05 Oct 2023

Keywords

Metasurface
Polarization
Conversion Ratio
Polarization Converter
Ultrathin

Abstract

Reflective polarization conversions with a simplistic design of an ultrathin, single-layered, and multi-functional anisotropic metasurface as a polarization converter is utilized for Ku- and K-band applications. The designs with two substrate thicknesses ($0.095\lambda_0$ and $0.069\lambda_0$, respectively) are capable of a cross-polarization converter (CPC) and a linear-to-circular (LTC) polarization conversion. The design with $0.095\lambda_0$ thickness achieves a CPC between 17.96 and 26.90GHz with the efficiency of more than 90% and a relative bandwidth of 40% under normal incidence. It maintains angular stability by altering the oblique incidence angles up to 30^0 with greater than 80% of the PCR in the K-band. Meanwhile, an LTC in two frequency bands, 10.30-10.53GHz and 28.65-29.70GHz, is also numerically demonstrated. The second design with $0.069\ \lambda_0$ thickness provides a CPC above the PCR value of 87% in the frequency range from 10.46-23.05GHz (covering the entire Ku- and part of the K-band) with angular stability of 40 above the PCR value of 80%. In the meantime, an LTC with relative bandwidth of 75% in the frequency range from 9.53-9.79&24.74-25.27GHz is numerically revealed. These polarization converters exhibit relatively good performances of facile structure and multi-functional properties, which can be useful in Ku- and K-band applications.

1. INTRODUCTION

Polarization is fundamental/critical parameter of electromagnetic (EM) waves in arising range of polarization-sensitive devices& applications, including beam splitters, wave plates, and antennas, gain enhancement of an antenna as well as reduction of EM interference and radar cross-section (RCS) [1–8]. Therefore, there has been an interest in researching new designing and approaches to regulate& manipulate the polarization of EM waves. For this reason, controlling the status of this vital feature of EM waves has found a place among the more critical study topics.

Conventional techniques, as the Faraday effect, are the solutions to control polarization [9, 10]. However, the limitations of these techniques are directly related to bulky size, narrow bandwidth, and the response against angle incidence, resulting in the disadvantages of traditional techniques in practical applications. Despite these limitations, the designs and applications of metasurfaces that can control the electric& magnetic responses in the EM wave-material interaction offer an excellent remedy. Therefore, designing a polarization converter (PC) based on metasurfaces with a facile structure& size, large bandwidth, and decent performance with better angular stability is still challenging. By altering the material properties or the metasurface's size and geometry, artificial 2D planar metasurfaces suggest possible methodologies controlling the polarization of EM waves [9, 11, 12].

*e-mail: ahmetteber@bayburt.edu.tr

In this regard, polarization conversion has been utilized as single-layer [13–15] and multilayer [16–18] in microwave [19–21], terahertz [22–25], infrared [26–28], and visible [14, 29] frequency regions. Based on these frequency regions, there exist modes providing easy polarization regulation of the incoming EM wave, such as reflection and transmission modes. Although these modes have various advantages trading off each other, transmission mode is generally used in multi-layer structures and has a cost, time wastage, and production difficulties [4]. However, polarization converters operated with reflection mode are more practical and straightforward because they can be applied in a single layer thanks to their metal-dielectric substrate material-metal structure. PCs working in reflective mode can be additionally provided a higher bandwidth than PCs operating in the mode of transmission and are more prevalent in the literature. More recent, the development of multi-functional polarization converters has been studied as converters of cross-polarization (CPC) [30–33], linear-to-linear (LTL) [34–36], linear-to-circular (LTC) [37–39], circular-to-circular (CTC) [40, 41], minimizing the dimensions and reducing complexity and manufacturing cost.

This work proposes a simple, easy-to-implement ultrathin, single-layered, multi-functional polarization converter for Ku- and K-band applications. The performance of the polarization conversion and operation principle are thoroughly examined. In addition, all investigations are operated for the substrate thickness as 0.095 λ_0 and 0.069λ_0, respectively. We obtained linear cross-polarization conversion for both thickness values with efficiencies above 90% and 87%, respectively. We also observed that LTC polarization conversion occurs. The changes in the substrate thickness allow the operating band and bandwidth to be tuned.

2. METASURFACE STRUCTURE AND METHODOLOGY

2.1. Design of Structure

The design parameters of the metasurface as a polarization converter are projected (Figure 1).

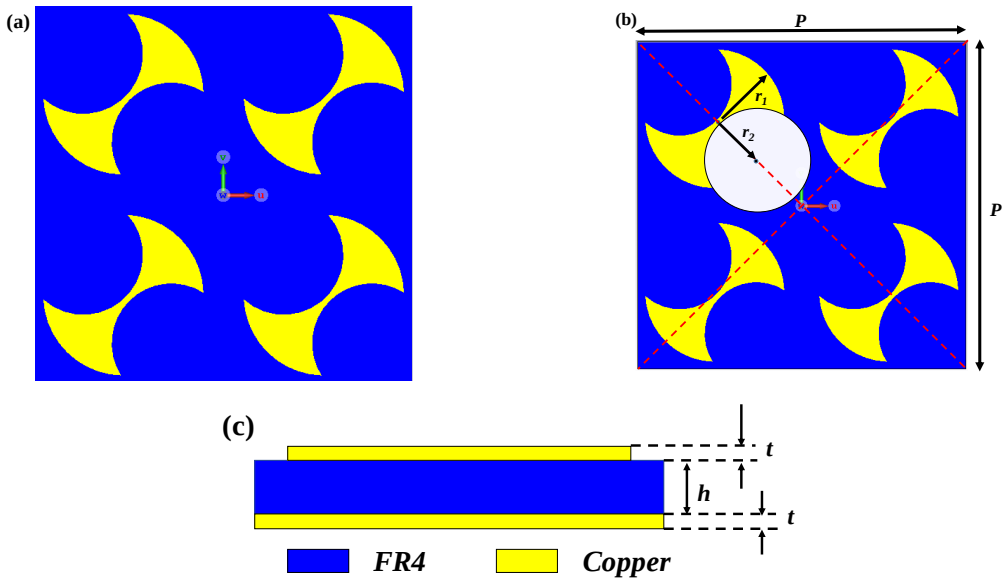

Figure 1. *Schematic of suggested polarization converter. (a) Top surface view. (b) Top surface view including design parameters. (c) Side view*

As known, geometric parameters must be carefully optimized for the best configuration, the host matrix, size, shape, etc., to obtain reasonable polarization conversion properties. In the converter structure, a periodic anisotropic metasurface array is used. The structure has four identical double-sided axes (DSA) with a thickness of 35µm on the top surface as a diagonally symmetric view, At the same time, the bottom part of the substrate (FR-4) is entirely covered by the copper plate with a thickness (t) of 35µm and a conductivity (σ) value of 5.86×10^{-7} S/m. In the beginning, the first DSA at the center points of O_1(-2.5, 2.5)

is created as a circular plate with a diameter of 2mm. Then, two identical circular plates are subtracted from the central circular plate at the center points of O_1(-1.3,1.3) and O_2(-3.5,3.5). After that step, we copied and transformed this created DSA at the direction of the y-axis by -5mm, resulting in the second DSA. The third DSA is also created when the first DSA is transformed simultaneously at the direction of the x-axis by 5mm and the y-axis by -5mm. The last DSA is transformed at the direction of the x-axis by 5mm and the y-axis by 5mm simultaneously. In this way, the unit cell design is obtained. FR-4 substrate material used in this study has a thickness (h) of 1.6mm, including ε_r=4.3 as a relative dielectric constant and tan(δ_ε)=0.025 as a dissipation factor value. After the design parameters are optimized, the polarization converter obtained by the best design parameters is given by P=9.8mm, h=1.6mm, r_1=2mm, r_2=1.49mm, as shown in Figure 1.

2.2. Method and Reflection Coefficients

The polarization conversion efficiency of a linear PC can be predicted by the polarization conversion ratio (PCR). In Equation (1) [7, 42], the following formula can be used to determine PCR, assuming that the polarization of the incident wave field is at the direction of the y-axis. Similarly, if a polarization of incident wave field is in the x-direction, the x- and y-subscripts are exchanged in this formula to be applied [43]

$$PCR = \frac{\left|r_{xy}\right|^2}{\left|r_{xy}\right|^2 + \left|r_{yy}\right|^2} \tag{1}$$

where r_{xy} and r_{yy} are the reflection coefficients (RCs). $r_{xy} = \left|E_{rx}\right| / \left|E_{iy}\right|$ is the cross-polarization reflection coefficients, while $r_{yy} = \left|E_{ry}\right| / \left|E_{iy}\right|$ is the co-polarization reflection coefficient. *E* implies the electric field (EF) here, while *i* and *r*, respectively represent the incident and the reflected electromagnetic (EM) waves. If the designed unit cell is diagonally symmetrical, the co- and cross-polarized reflection waves are similar in magnitude and phase when the incident wave is along the x- and y-axis. Namely, the RCs of the reflected field E_r for the x-polarized incident electric field are written for co- and cross-polarized components as $r_{yx} = \left|E_{ry}\right| / \left|E_{ix}\right|$ and $r_{xx} = \left|E_{rx}\right| / \left|E_{ix}\right|$. From this perspective, the best way to evaluate a circular polarization converter's ability to sustain circular polarization is by using the polarization-maintaining ratio (PMR). When the reflected wave is a right-handed circularly polarized (RHCP) wave, the PMR can be written as the following formula [32]:

$$PMR = \frac{\left|r_{++}\right|^2}{\left|r_{-+}\right|^2 + \left|r_{++}\right|^2} \tag{2}$$

where + signifies a RHCP, while - denotes a left-handed circular polarization (LHCP) circumstances. The subscripts + and – are exchanged in Equation (2) for an LHCP wave. Any reflected EM wave from a metasurface typically has two field components. The first one is a co-polarized reflected field with the same polarization as the incident wave. The other is a cross-polarized reflected field, known as orthogonal component of incident polarization. The Jones reflection coefficient matrix **R** [4] in the Cartesian coordinates is mathematically utilized to analyze co- and cross-polarizations:

$$R = \begin{bmatrix} R_{xx} & R_{xy} \\ R_{yx} & R_{yy} \end{bmatrix}. \tag{3}$$

The following formula is used to understand the relationship between the linear and the circular polarization in the incident and the reflected wave [44, 45]:

$$R_{CP}=\begin{bmatrix} R_{++} & R_{+-} \\ R_{-+} & R_{--} \end{bmatrix}=\frac{1}{2}\begin{bmatrix} (R_{xx}-R_{yy})-i(R_{xy}+R_{yx}) & (R_{xx}+R_{yy})+i(R_{xy}-R_{yx}) \\ (R_{xx}+R_{yy})-i(R_{xy}-R_{yx}) & (R_{xx}-R_{yy})+i(R_{xy}+R_{yx}) \end{bmatrix} \quad . \tag{4}$$

Note that the RCs of linear polarization are represented with the notation of R_{ab} (where *a, b = x, y*) while the RCs of circular polarization are notated as R_{ab} (where *a, b*= +, -) through the Equation (4).

For further investigation, it is important to understand whether the reflected wave is RHCP or LHCP. Therefore, Stokes parameters are utilized to obtain the normalized ellipticity, $e=S_3/S_0$, as following [46]

$$S_0=\left|R_{xy}\right|^2+\left|R_{yy}\right|^2 \tag{5}$$

$$S_1=\left|R_{yy}\right|^2-\left|R_{xy}\right|^2 \tag{6}$$

$$S_2=2\left|R_{xy}\right|\left|R_{yy}\right|\cos\Delta\Phi \tag{7}$$

$$S_3=2\left|R_{xy}\right|\left|R_{yy}\right|\sin\Delta\Phi \tag{8}$$

where $\Delta\Phi=\Phi_{yy}-\Phi_{xy}$ with Φ_{yy} and Φ_{xy} are the reflection phases for co- and cross-polarization, respectively. There exist two options regarding *e*-value as ±1. When *e* = +1, the reflected wave is RHCP while the reflected wave is LHCP for e = -1. For the first option of *e*=+1, $\left|R_{xy}\right|=\left|R_{yy}\right|$, $\Delta\Phi=-90^0+2k\pi$, and the reflected wave is RHCP. For the second option of e = -1, $\left|R_{xy}\right|=\left|R_{yy}\right|$, $\Delta\Phi=90^0+2k\pi$, and the reflected wave is an LHCP. k is an integer for both circumstances.

3. RESULTS AND DISCUSSION

3.1. Simulation Outcomes

Simulations were performed by CST Microwave Studio to analyze PCR efficiency and other parameters of ellipticity (e), magnitude, phase by incidence angle. Based on different values of normal incidence, the reflection coefficients are also examined via the different polarization angles. By automatically selecting the number of networks per unit wavelength, tetrahedral network type analysis was performed in the selected frequency band. We performed all simulations in the broader frequency range rather than the frequency spectrum under focus (18-26.5GHz). For the incoming y-polarized wave under normal incidence, the numerical results are presented in Figure 2. The magnitude of $\left|\mathbf{R}_{xy}\right|$ is higher than 0.9 whereas $\left|\mathbf{R}_{xy}\right|$ is the cross polarization coefficient. Meanwhile, the co-polarization coefficient ($\left|\mathbf{R}_{yy}\right|$) is below 0.3 in the frequency range of 17.96-26.90GHz (Figure 2a). It is also observed that the reflected wave of y-polarized incoming wave has the same magnitudes ($\left|\mathbf{R}_{xy}\right|=\left|\mathbf{R}_{yy}\right|$) of 0.65 at 10.42 and 29.24 GHz, whereas the PCR value is 0.5, as represented in Equation (1), while the phase differences in Figure 2b are approximately $+90^0$ and $+270^0$ at the corresponding frequencies. In Figure 2b, the phase information of reflection wave is represented. According to Figure 2b, the magnitude of the co- and cross-polarized RCs has the same value, while their phase difference is multiplied by an odd number of 90^0 at 10.42 and 29.24 GHz. Thus, the linearly polarized incoming wave is reflected in circularly polarized wave form. The PCR under normal incidence is simulated in the Figure 2c. For our focus frequency range, the converter has a PCR value above 0.9 in the frequency range of 17.96GHz to 26.90GHz, which entirely covers the K-band. In addition, the ellipticity value (*e*) shown in Figure 2c reaches unity value (+1) at the frequency of 10.42GHz and -1 at the frequencies of 29.24GHz when $\left|R_{xy}\right|=\left|R_{yy}\right|$. It means that the suggested converter works as a RHCP at

10.42GHz while it operates as a LHCP at 29.24GHz. The efficiency of a circular polarization converter can be predictable if the magnitude ratio of ($|E_{co}|/|E_{cross}|$)co- and cross-polarized reflection fields is in the range of 0.85-1.15 and phase differences should be in the range from $n90^0 \pm 5^0$ where n is an odd number [45]. Therefore, the proposed converter shown in the inset of Figure 2d shows the circular polarization conversion between 10.30-10.53GHz and 28.65-29.70GHz.

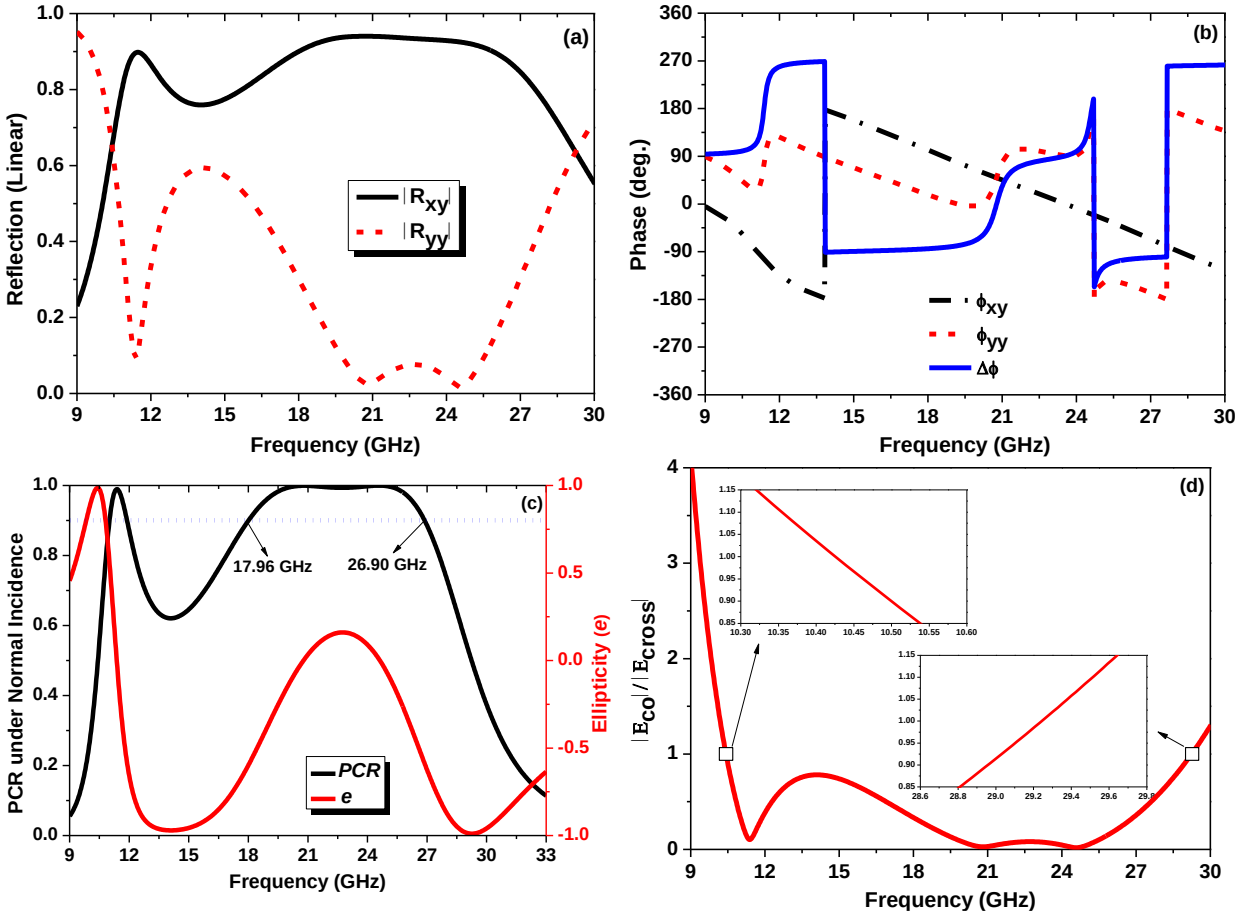

Figure 2. *(a) Magnitude of co- and cross-polarized RCs. (b) Phases and phase difference of co- and cross-polarized RCs. (c) PCR under normal incidence for y-polarization and Ellipticity (e). (d) The magnitude ratio of the co- and cross-polarized reflected fields of the proposed polarization converter under normal incidence for y-polarization*

3.2. Theoretical Analysis

To comprehend the cross-polarization conversion, an examination of the eigen-polarizations and -values for the suggested PC should be demonstrated. The eigen-polarizations and the eigenvectors are obtained as follows:

$$\boldsymbol{RX} - \boldsymbol{mX} = 0 \tag{9}$$

where $\boldsymbol{X}$ is the eigenvector and m is the eigenvalue. It should be noted that the ideal condition is assumed, namely cross-polarized reflections are not considered. At resonant frequencies from Figure 1a, $|\mathbf{R}_{xx}| = |\mathbf{R}_{yy}| \approx 1$ and $|\mathbf{R}_{xy}| = |\mathbf{R}_{yx}| \approx 0$ are roughly obtained. When these values put into Jones reflection coefficient matrix, the coefficient matrix is obtained as follows:

$$R=\begin{bmatrix}0 & 1\\ 1 & 0\end{bmatrix} \tag{10}$$

where $\boldsymbol{u}=(1\ 1)^T$ and $\boldsymbol{v}=(-1\ 1)^T$ with the independent eigenvalues of $e^{i0}=1$ and $e^{i\pi}=-1$, respectively, are the linearly independent eigenvectors. It means that u- and v-polarized incoming waves are reflected without any cross-polarization conversion. The reflected wave has unity magnitude and 0^0 and 180^0 phases, respectively. Since cross-polarization conversion does not occur at u- and v-directions, $\left|\mathbf{R}_{uu}\right|=\left|\mathbf{R}_{vv}\right|\approx 1$ and $\left|\mathbf{R}_{uv}\right|=\left|\mathbf{R}_{vu}\right|\approx 0$.

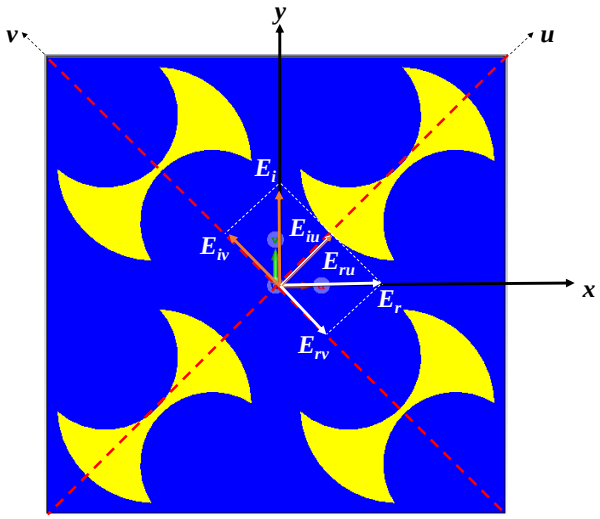

Figure 3. *Orthogonal components in the u- and v-direction*

Assuming that incoming wave EM wave (E_i) is at the y-direction, the orthogonal components (u- and v-) are inclined to y-axis with 45^0 and -45^0, respectively. So, the incoming wave (E_i) and the reflected wave (E_r), respectively is written [45] as

$$E_i=\hat{y}E_i=\hat{u}E_{iu}+\hat{v}E_{iv} \tag{11}$$

$$E_r=\hat{u}E_{ru}+\hat{v}E_{rv}=\hat{u}r_uE_{iu}+\hat{v}r_vE_{iv} \tag{12}$$

where $\hat{u}$ and $\hat{v}$ are the unit vectors while r_u and r_v are the complex RCs in the u- and v-directions, respectively. Khan and colleagues proposed the equation below:

$$E_r=\hat{u}(r_{uu}E_{iu}e^{i\Phi_{uu}}+r_{uv}E_{iv}e^{i\Phi_{uv}})+\hat{v}(r_{vv}E_{iv}e^{i\Phi_{vv}}+r_{vu}E_{iu}e^{i\Phi_{vu}}) \tag{13}$$

where r_{uu}, r_{uv}, r_{vv}, and r_{vu} are the magnitude of co- and cross-RCs while Φ_{uu}, Φ_{uv}, Φ_{vv}, and Φ_{vu} are the phases of co- and cross-RCs in the u- and v-axis, respectively.

The asymmetrical structure of the metasurface may exhibit anisotropic properties on the presented polarization converter, depending on the relative permittivity and permeability. As a result, there may be variations in the phase and the magnitude of the reflected waves. When $\left|\mathbf{R}_{uu}\right|=\left|\mathbf{R}_{vv}\right|\approx 1$, $\left|\mathbf{R}_{uv}\right|=\left|\mathbf{R}_{vu}\right|\approx 0$, and $\Delta\phi=\phi_{uu}-\phi_{vv}=\pm 180^0+2k\pi$ (k is an integer)[47], the synthetic fields of E_{ru} and E_{rv} will be at the x-direction (Figure 3). Thus, the incoming polarized wave rotates 90^0, resulting in CPC conversion. If $\Delta\phi=\phi_{uu}-\phi_{vv}=\pm 90^0+2k\pi$ (k is an integer), then, LTC conversion can be attained.

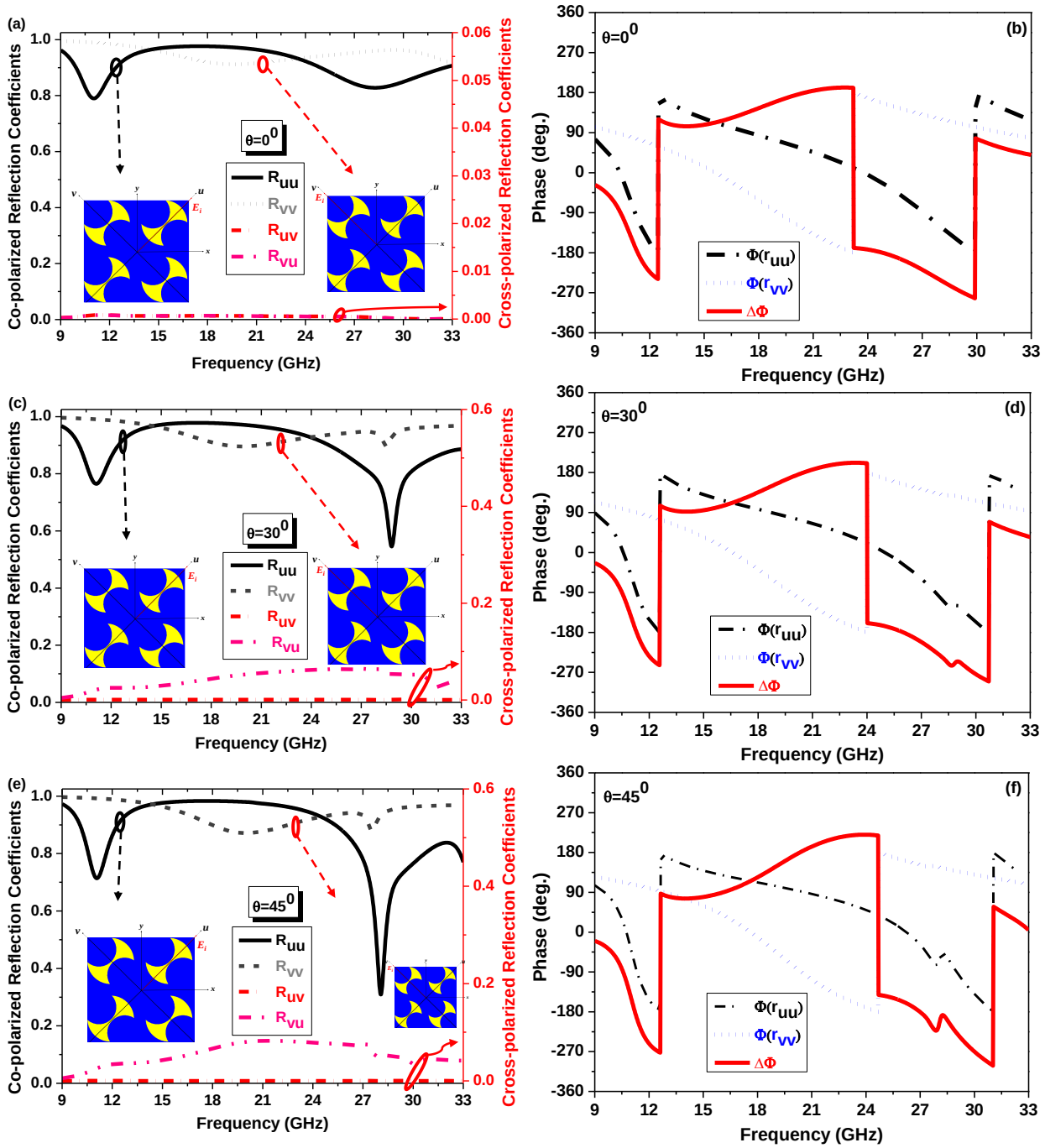

Figure 4. *(a, c, e) The magnitude and (b, d, f) The Phases of the RCs of u- and v- components for the suggested PC at the 0^0, 30^0, and 45^0 incidences*

From this perspective, the magnitude and the phase of the RCs of the orthogonal-components for the incidence angles of 0^0, 30^0, and 45^0 are simulated to assess the property of the proposed converter, as shown in Figure 4. For all circumstances, the magnitude of the cross-polarized RCs is nearly 0. The co-polarized RCs are roughly equal to 1 in K-band. Moreover, the phase differences between the u- and u-polarized wave (reflected ones) is roughly $+180^0$ or -180^0 in the K-band, which indicates the suggested converter reveals the linear cross-polarization conversion. Meanwhile, phase difference is approximately -90^0 or -270^0, which implies the suggested converter reveals LTC conversion at 10.30-10.53GHz and 28.65-29.70GHz.

3.3. Surface Current Distributions

The surface current distributions for the top and bottom surface layers at the resonance frequencies of 11.39GHz, 20.82 GHz and 24.60GHz are examined to understand the principles under the conversion mechanism for further step (Figure 5).

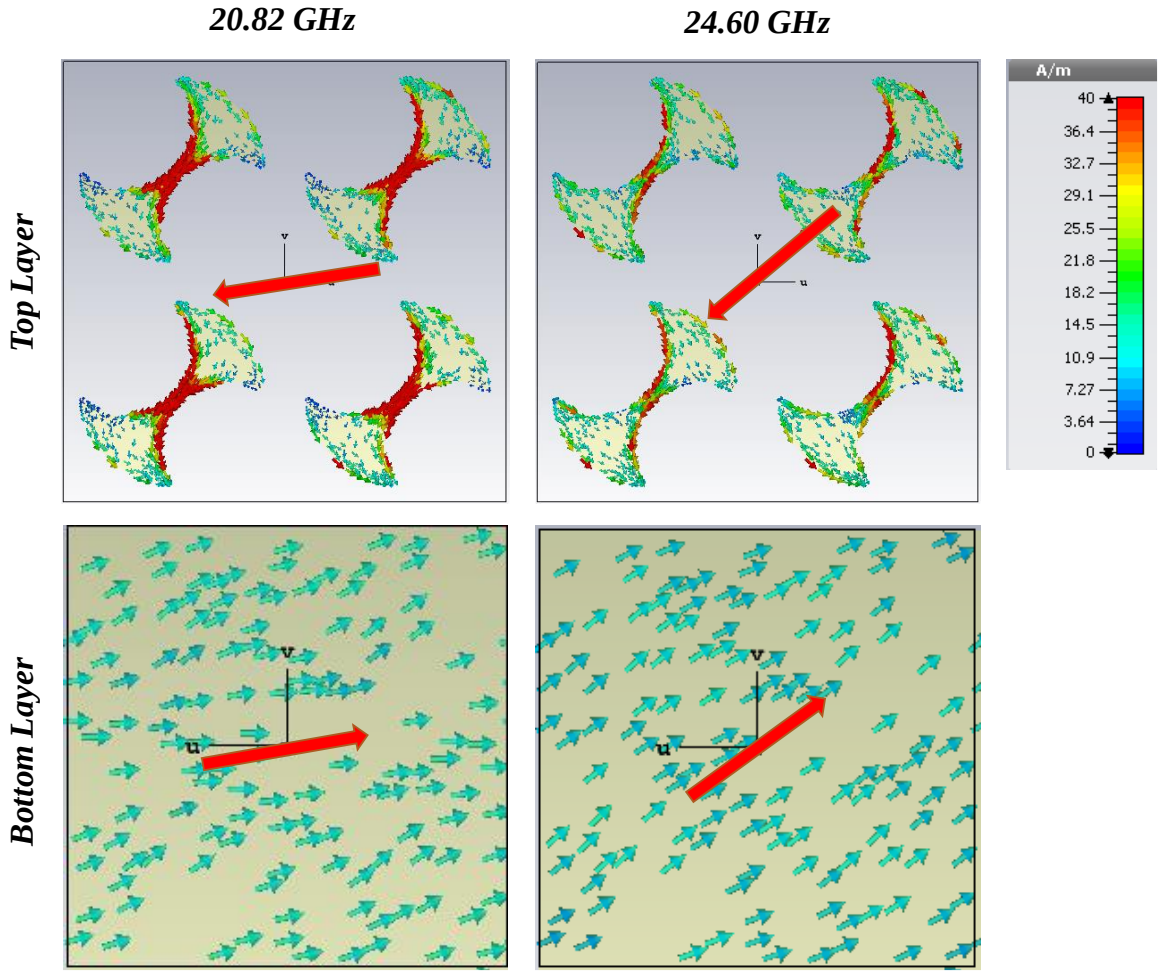

Figure 5. *The surface current distributions over the frequency band analyzed on the top and the bottom layer of the metasurface for the resonant frequencies*

Since the resonant frequency of 11.39GHz is not in the K-band range, the surface current distribution is not examined, here. Due to several interactions between meta-atoms and the incident EM wave, electrically and magnetically polarized meta-atoms are formed. This leads to bi-anisotropy electric&magnetic dipole moments of the metasurface. The relationship between incident fields and regionally averaged effective dipole moments is shown by Equation (14)

$$\begin{bmatrix} p \\ m \end{bmatrix} = \begin{bmatrix} P_{ee} & P_{em} \\ P_{me} & P_{mm} \end{bmatrix} \begin{bmatrix} E \\ H \end{bmatrix}. \tag{14}$$

Here, $p=\begin{bmatrix} p_x \\ p_y \end{bmatrix}$ and $m=\begin{bmatrix} m_x \\ m_y \end{bmatrix}$ are the electric and the magnetic dipole moments. Also, $E=\begin{bmatrix} E_x \\ E_y \end{bmatrix}$ and $H=\begin{bmatrix} H_x \\ H_y \end{bmatrix}$ are the electric and the magnetic fields while p_{em} implies the electric-magnetic polarizability. The effective surface impedance is clarified using these dipole moments, illustrated as $Z(\omega)=\sqrt{\mu(\omega)/\varepsilon(\omega)}$ where $\mu(\omega)$ and $\varepsilon(\omega)$ are the permeability and the permittivity as a function of frequency, respectively. By this explanation, reflection coefficient $R(\omega)$ can be written by the effective surface impedance under normal incidence:

$$R(\omega)=\frac{Z(\omega)-Z_0}{Z(\omega)+Z_0} \tag{15}$$

where $Z_0(=377\Omega)$ is free space impedance. When the effective surface impedance is much higher than the free space's impedance ($Z(\omega_r)\gg Z_0$), the reflection coefficient $R(\omega)$ is equal to 1 where ω_r is the resonant frequency. It is necessary to investigate the surface current that the time-varying dipole moments produce. It is possible to characterize the relationship between electric and magnetic field densities and current densities over the polarization effect as follow [43]:

$$\begin{bmatrix} J \\ M \end{bmatrix}=i\omega\begin{bmatrix} P_{ee} & P_{em} \\ P_{me} & P_{mm} \end{bmatrix}\begin{bmatrix} E \\ H \end{bmatrix} \tag{16}$$

where $J=\left[J_x, J_y\right]^T$ and $M=\left[M_x, M_y\right]^T$ are the electric and the magnetic current densities, respectively. The notation of P_{ee}, P_{mm}, P_{em}, and P_{me} represent the self- and associated electric and magnetic polarizations where ω is the angular frequency. As shown in Figure 5, the incoming EM wave persuades surface currents in the inner and outer curved sections of the suggested metasurfaces due to the anisotropy of its top surface. The surface currents on both layers are in opposed directions, so that it can be said that the magnetic resonance is responsible behind the physical mechanism.

3.4. Parametric Investigations

The optimization parameters of designation are shown in Figure 6. As mentioned regarding the geometric parameters before, the magnitude and the resonant frequencies can be editable by the geometry, dimensions, thickness, and structure properties. With that manner, the optimization process what we have done in this study is carried out obtaining the best polarization conversion ratio (PCR) by modifying the size (P), the thickness of the substrate (h), and the radius of subtracted circular plates (r_1 and r_2) of the metasurface.

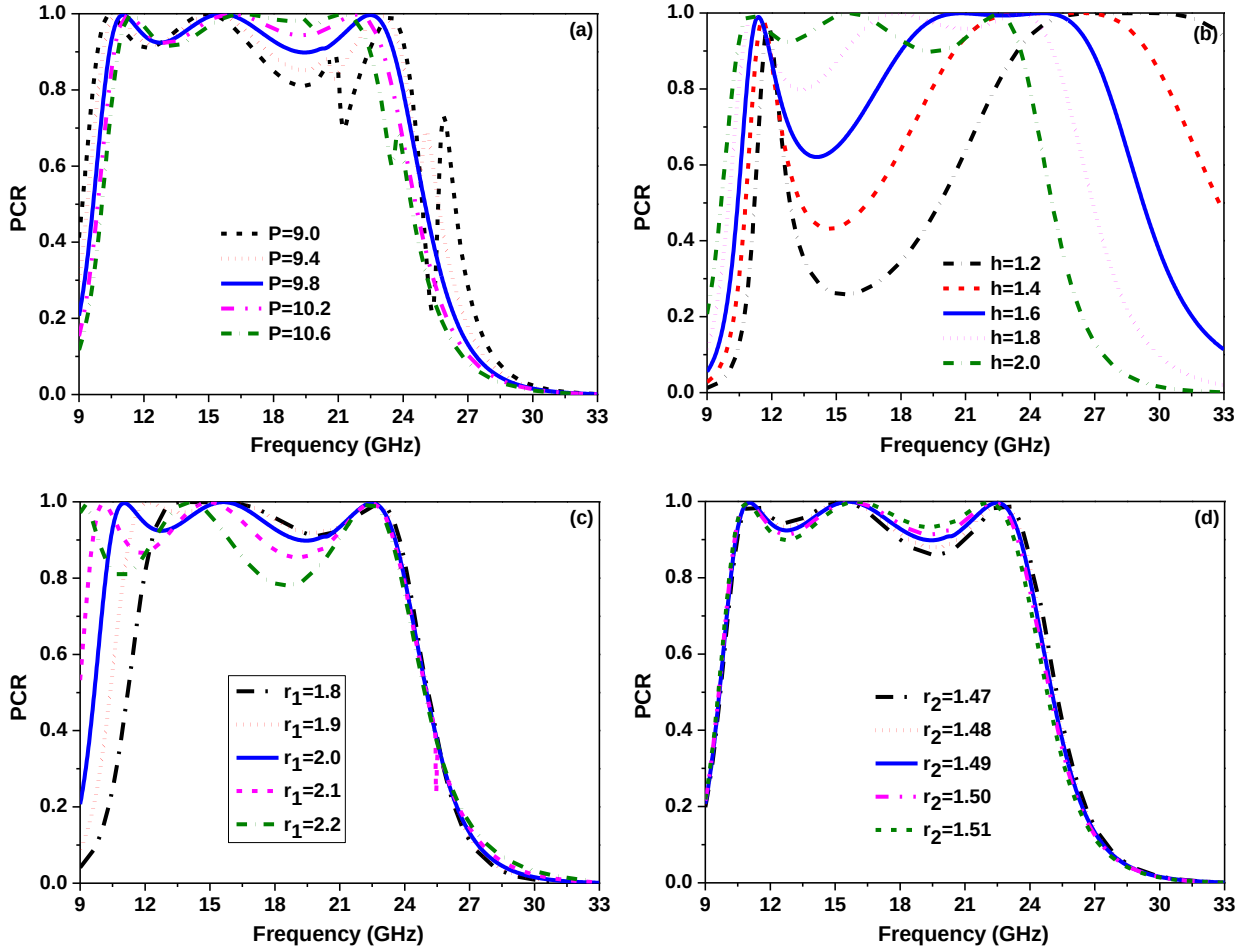

Figure 6. *Parametrical Investigation. (a) Size of the design, P. (b) The thickness of substrate, h. (c) DSA radius, r_1. (d) Radius of the subtracted circular plates, r_2*

In the practical applications, oblique angular stability of a PC should be considered. Figure 7 presents the relation between PCR and oblique angle to understand angular stability for TE and TM mode. The PCR can be maintanined above 0.8 in the frequency range from 17.96-26.90 GHz with the incidence angle up to 30^0 (Figure 7).

It is also investigated that the frequency dependent PCR for TE and TM modes according to the incidence angle as illustrated in Figure 7a, b and 7c, d, respectively. The PCR values are approximately identical for these modes under normal incidence of EM wave (Figure 7e).

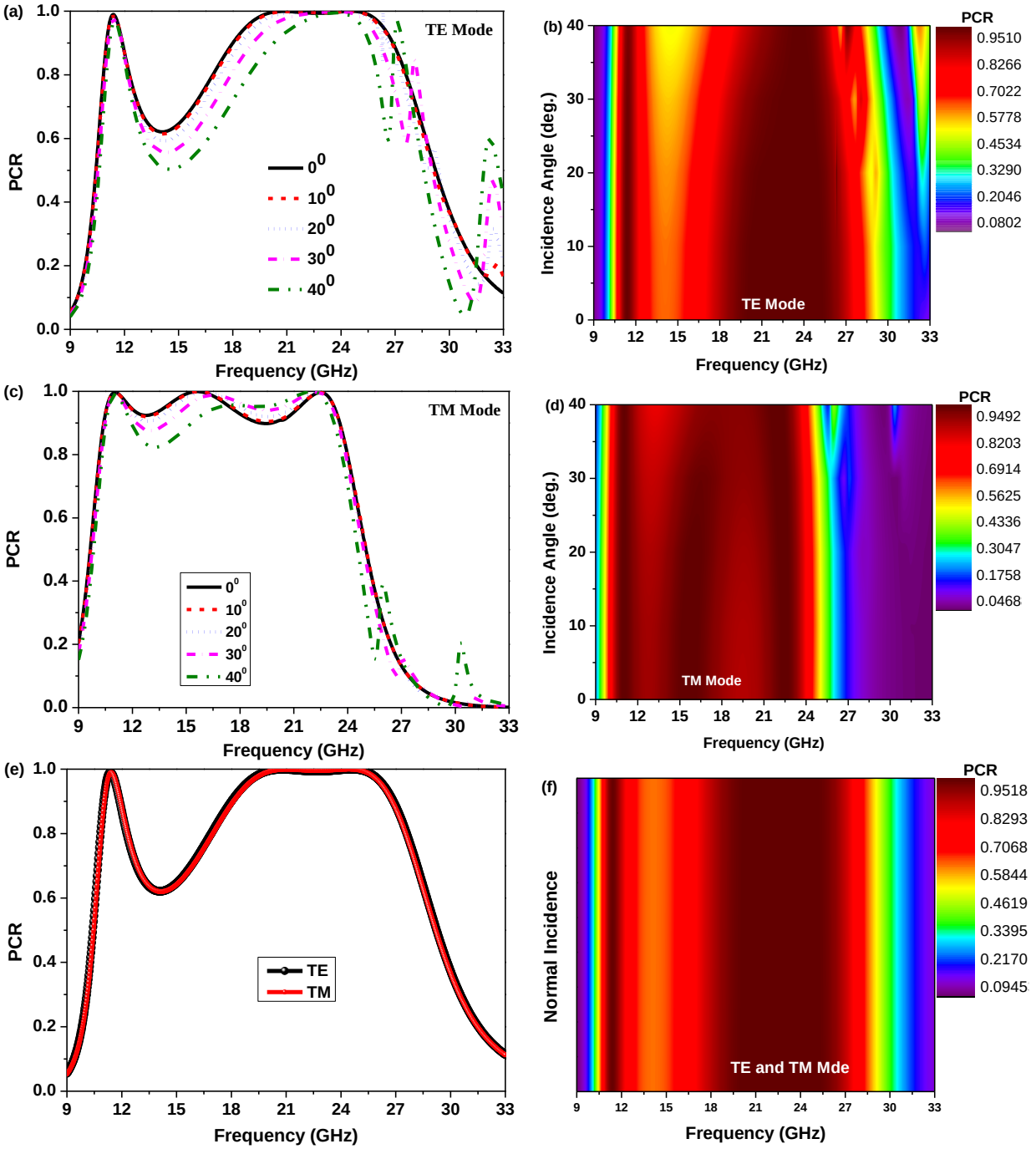

Figure 7. *Based on incidence angle, (a) PCR for TE Mode. (b) Contour plot of PCR for TE Mode. (c) PCR for TM Mode. (d) Contour plot of PCR for TM Mode. (e) PCR for TE and TM Modes. (f) Contour plot of PCR for TE and TM Mode*

3.5. Performance Analysis of the Proposed Converter

In the parametrical investigations as shown in Figure 6b, when the thickness of the substrate h is 2mm, the PCR band shifted lower frequencies, covering the entire Ku-band and a part of K-band. Figure 8 reveals the simulated investigations for incidence y-polarized wave under normal incidence.

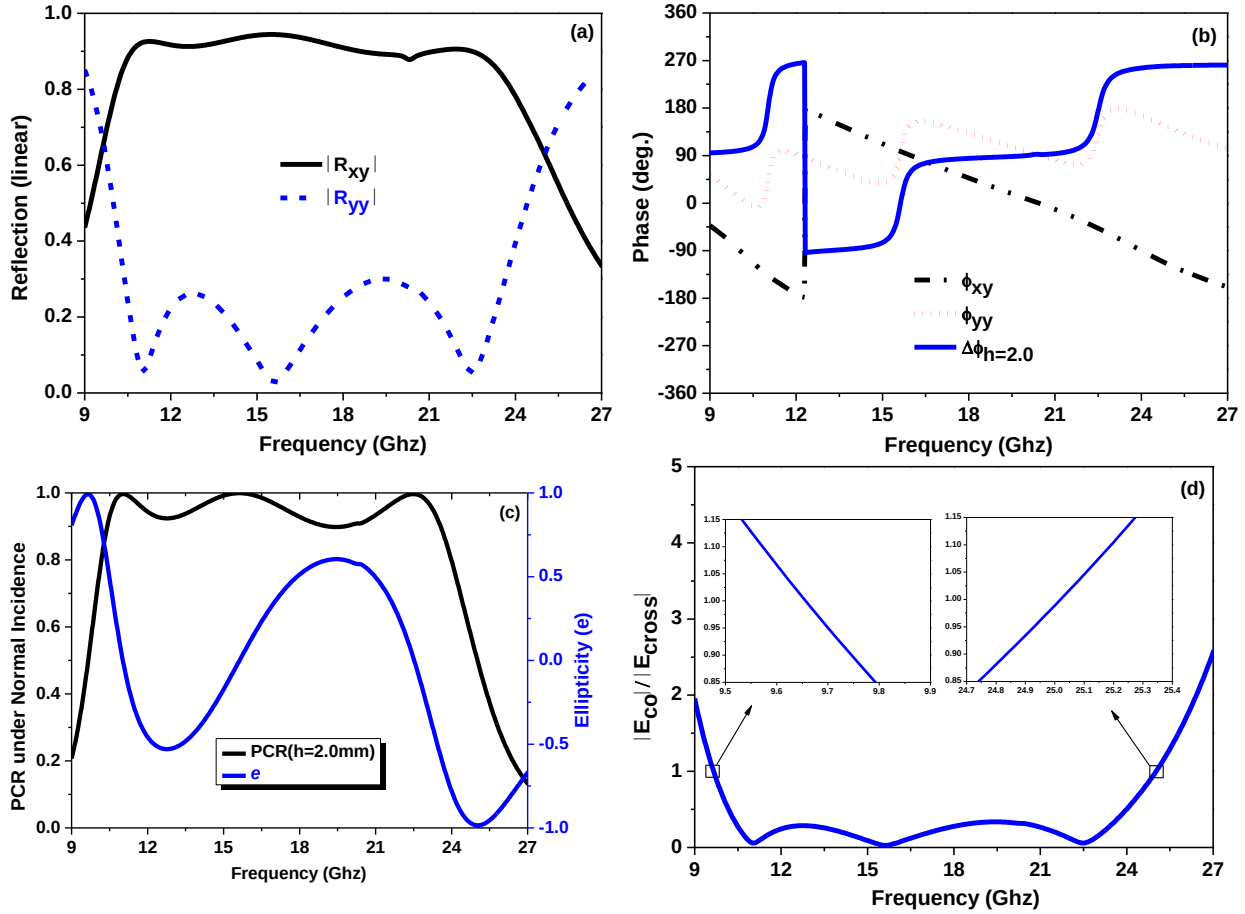

Figure 8. *For h=2.0mm: (a,b) Magnitude and phase of co- and cross-polarized RCs. (c) PCR under normal incidence for y-polarization and Ellipticity (e). (d) The* $|E_{co}|/|E_{cross}|$ *of the proposed polarization converter under normal incidence for y-polarization*

In Figure 8a, the magnitude of the cross-polarization coefficient (R_{xy}) is higher than 0.87, while the co-polarization coefficient (R_{yy}) is under 0.3 in the frequency range of 10.46-23.05GHz. Also, the incident y-polarized wave is reflected with approximately equal magnitudes (R_{xy}=R_{yy}) of 0.65 at 9.56GHz and 25.01 GHz, resulting in a PCR value of 0.46 as represented in Equation (1). The phase differences at these frequencies shown in Figure 8b are approximately $+90^0$ and $+270^0$. According to the same figure, the magnitude of the co- and cross-polarized reflection coefficients has the same value while their phase difference is an odd multiple of 90 degrees at 10.46GHz and 23.05GHz. Therefore, a linearly polarized incident wave is reflected as circularly polarized wave. The PCR under normal incidence shown in Figure 8c is above 0.87 in the frequency range of 10.46-23.05GHz, which is entirely cover the Ku-band and some part of K-band between 18GHz and 23.05GHz. In addition, the ellipticity value (e) shown in Figure 8c approximately attains unity value (+1) at 9.56 GHz while it approximately attains -1 value at 25.01GHz when R_{xy}=R_{yy}. It means that the proposed converter with the thickness of 2mm operates as a RHCP at 9.56GHz while it operates as a LHCP at 25.01GHz. In Figure 8d, according to the ratio of the magnitude of co-and cross-polarized reflection fields shown in the inset figure, the proposed converter with h=2mm exhibits circular polarization conversion in the frequency ranges of 9.53-9.79GHz and 24.74-25.27GHz.

For the practical applications, the behavior of the polarization converter should be investigated based on obliquely incident angle. Figure 9 presents the magnitude of co- and cross-polarized RCs and PCR based on incidence angles ranging from 0^0 to 45^0 for TE polarization. As the incidence angle is increased, the magnitude of cross polarization reflection increases while the magnitude of co-polarization reflection decreases. However, in the operating frequency range of Ku- and part of K-band with incident angle up to 40^0, the PCR is maintained above 0.8.

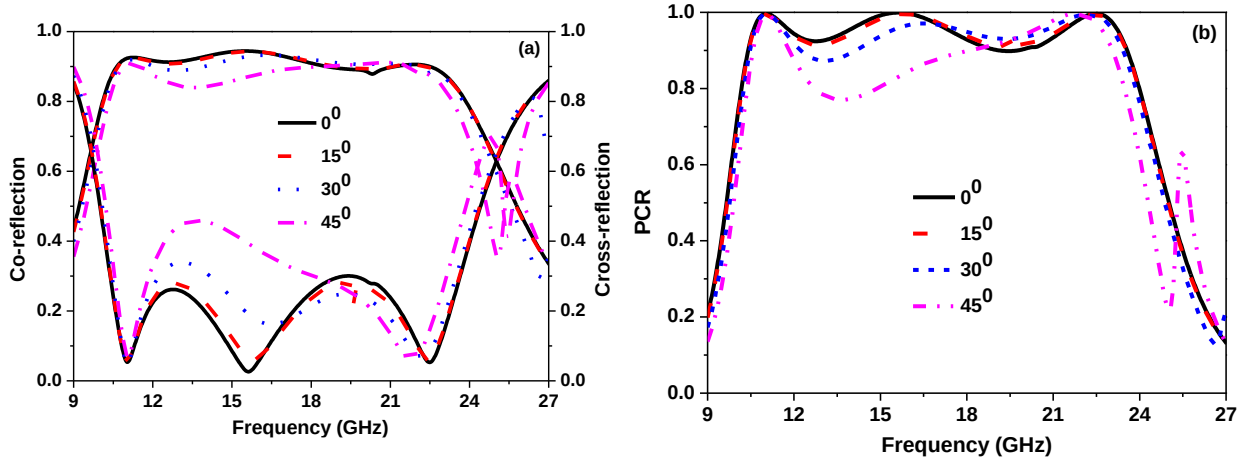

Figure 9. *For h=2.0mm: (a) Magnitude of co- and cross-polarized RCs. (b) PCR of the suggested polarization converter based on incidence angles at TE polarization*

Figure 10a and 10b illustrate the magnitude and phase variations of R_{uu}, R_{vv} and Phase difference, respectively. The magnitudes of the co- polarized RCs of R_{uu} and R_{vv} have magnitudes larger than 0.8 in the operated frequency range. In addition, the magnitudes of cross polarized reflection coefficients of R_{uv} and R_{vu} are almost zero as shown in Figure 10a. The phase difference between the u- and v-polarized wave in the working frequency band is roughly $+180^0$ or -180^0, which indicates the designed converter displays the linear cross-polarization conversion. On the other hand, the phase difference is approximately $+90^0$ or -270^0, which implies that the proposed converter shows LP-to-CP conversion at 9.53-9.79GHz and 24.74-25.27GHz.

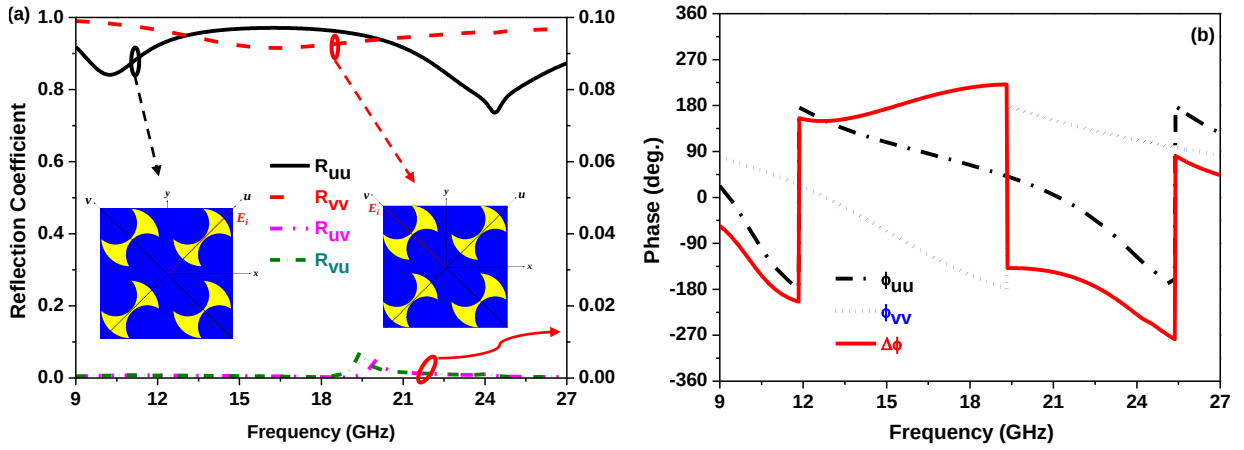

Figure 10. *(a) The magnitude and (b) The Phases of the RCs of u- and v- components for the proposed polarization converter at TE mode under normal incidence*

It is obviously seen that the operated frequency range is substrate thickness dependent in Figure 11. When the substrate thickness increased from 1.6mm to 2mm, the operated band shifted Ku- and part of K-band up to 23.05GHz. From this perspective, it can be said that our design has ability to control operated frequency band.

The relative bandwidth belongs to the proposed converter is calculated by using the formula of $BW = 2(f_u - f_L)/(f_u + f_L)$. According this formula, f_u is the highest frequency value of the operated frequency band while f_L is the lowest frequency value of the operated frequency band. As a result, for h=1.6mm or $0.095\lambda_0$, BW is obtained as 30 above PCR value of 0.8 while the BW is 40 above the PCR value of 0.8 for h=2mm or $0.069\lambda_0$.

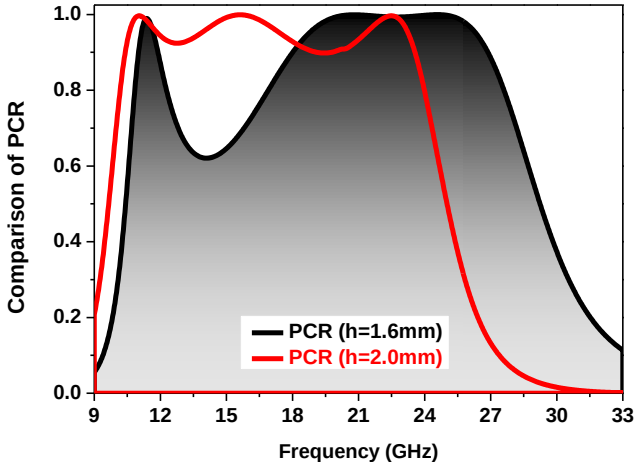

Figure 11. *The comparison of PCR at TE mode under normal incidence for h=1.6mm and h=2.0mm*

For our performance analysis, we also compared the polarization characteristics of our design with some other published papers in the literature. The comparison conditions of operated frequency bands for linear to circular polarization conversion, for circular polarization conversion, and the substrate thickness are shown in Table 1.

Table 1. *Performance comparison*

Ref. No	Operating Bandwidth [GHz]	Conversion Type	Thickness [mm]	Angular stability [deg.]	PCR	Operated Band Name	Relative Bandwidth (RBW)
[4]	17.87-43.15	CPC	$0.070\lambda_0$	40 above 75%	Above 0.9	K-, Ka- and V-band	83%
	16.23-16.74&48.6-48.8	LP-to-CP					N/A
[42]	13.8-40.7	CPC	$0.092\lambda_0$	40 above N/A	Above 0.97	Ku-, K- and Ka-band	98.7%
[44]	8.77-24.71	CPC	$0.087\lambda_0$	N/A	Above 0.95	Most part of X-, Ku-, and most part of K-band	95.2%
[46]	10.42-16.72	CPC	$0.080\lambda_0$	45 above 90%	Above 0.9	Most part of Ku-Band	46.4%
	9.34-9.64&19.14-20.44	LP-to-CP		30 above 90%			N/A
[47]	12-18	CPC	$0.060\lambda_0$	45 above 80%	Above 0.9	Ku-band	40%
This work	**17.96-26.90**	**CPC**	**$0.095\lambda_0$**	**30 above 80%**	**Above 0.9**	**K-band**	**40%**
	10.90-10.53GHz & 28.65-29.70	**LP-to-CP**				**Part of X-band&part of Ka-band**	
	10.46-23.05	**CPC**	**$0.069\lambda_0$**	**40 above 80%**	**Above 0.87**	**Part of Ku-band and K-band**	**75%**
	9.53-9.79GHz & 24.74-25.27GHz	**LP-to-CP**				**Part of X-band&K-band**	

4. CONCLUSION

Reflection polarization conversion is obtained using two different models of the metasurface. The structures are simple, easy-to-fabricate, ultrathin, and multi-functional, utilizing Ku- and K-band. The impact of various structural characteristics is examined to evaluate the mechanism of polarization conversion. The changes in the substrate thickness provide that this structure can have the ability to switch the operated frequency band with an improvement of the bandwidth. For the first design, cross-polarization conversion are obtained more than 90% efficiency with angular stability of 30^0 between 17.96 and 26.90GHz. In comparison, the second design has 87% efficiency with angular stability of 40^0 in the operating frequency range of 10.46-23.05GHz. For both designs, linear-to-circular polarization conversion is also generated. As the subject of another study, one of these designs can be produced with a modular 3D engraving machine, especially the design with a substrate material thickness of $0.095\lambda_0$. PCB boards of this thickness are readily available on the market. Eventually, these simulated polarization converters reveal good performance, which is helpful in Ku- and K-band applications.

CONFLICTS OF INTEREST

No conflict of interest was declared by the author.

REFERENCES

[1] Ren, J., Jiang, W., Zhang, K., Gong, S., "A high-gain circularly polarized fabry-perot antenna with wideband Low-RCS property", IEEE Antennas and Wireless Propagation Letters, 17(5): 853–856, (2018).

[2] Zhang, L., Liu, C., Ni, C., Kong, M., Wu, X., "Low-RCS, Circular Polarization, and High-Gain Broadband Antenna Based on Mirror Polarization Conversion Metasurfaces", International Journal of Antennas and Propagation, 2019: 1-8, (2019).

[3] Veysi, M., Boyraz, O., Capolino, F., "A thin anisotropic metasurface for simultaneous light focusing and polarization manipulation", Journal of the Optical Society of America B, 32(2): 318-323, (2015).

[4] Coskun, A., Hasar, U.C., Ozmen, A., Ertugrul, M., Coskun, A., Hasar, U.C., Ozmen, A., Ertugrul, M., "Easy-to-Implement Ultra-Thin, Wide-Band, and Multi-Functional Polarization Converter for K and Ka Band Applications", Advanced Theory and Theory Simulations, 5(4): 2100543, (2022).

[5] Yuan, Y., Zhang, K., Ratni, B., Song, Q., Ding, X., Wu, Q., Burokur, S.N., Genevet, P., "Independent phase modulation for quadruplex polarization channels enabled by chirality-assisted geometric-phase metasurfaces", Nature Communications, 11(1): 1–9, (2020).

[6] Li, S.J., Cui, T.J., Li, Y.B., Zhang, C., Li, R.Q., Cao, X.Y., Guo, Z.X., "Multifunctional and Multiband Fractal Metasurface Based on Inter-Metamolecular Coupling Interaction", Advanced Theory and Simulations, 2(8): 1900105, (2019).

[7] Khan, M.I., Khalid, Z., Tahir, F.A., "Linear and circular-polarization conversion in X-band using anisotropic metasurface", Scientific Reports, 9(1): 1–11, (2019).

[8] Ako, R.T., Lee, W.S.L., Bhaskaran, M., Sriram, S., Withayachumnankul, W., "Broadband and wide-angle reflective linear polarization converter for terahertz waves", APL Photonics, 4(9): 096104, (2019).

[9] Nguyen, T.K.T., Nguyen, T.M., Nguyen, H.Q., Cao, T.N., Le, D.T., Bui, X.K., Bui, S.T., Truong, C.L., Vu, D.L., Nguyen, T.Q.H., "Simple design of efficient broadband multifunctional polarization converter for X-band applications", Scientific Reports, 11(1): 1–12, (2021).

[10] Lin, B., Guo, J., Lv, L., Wu, J., Ma, Y., Liu, B., Wang, Z., "Ultra-wideband and high-efficiency reflective polarization converter for both linear and circular polarized waves", Applied Physics A, 125(2): 1–8, (2019).

[11] Pouyanfar, N., Nourinia, J., Ghobadi, C., "Low-profile and high efficient artificial magnetic conductor metasurface for X-band applications", In 2020 28th Iranian Conference on Electrical Engineering (ICEE), Tabriz, Iran, 1-4, (2020).

[12] Khan, M.I., Tahir, F. A., "An angularly stable dual-broadband anisotropic cross polarization conversion metasurface", Journal of Applied Physics, 122(5): 053103, (2017).

[13] Wang, H. Bin, Cheng, Y.J., Chen, Z.N., "Wideband and Wide-Angle Single-Layered-Substrate Linear-to-Circular Polarization Metasurface Converter", IEEE Transactions on Antennas Propagation, 68(2): 1186–1191, (2020).

[14] Hu, Y., Ou, X., Zeng, T., Lai, J., Zhang, J., Li, X., Luo, X., Li, L., Fan, F., Duan, H., "Electrically Tunable Multifunctional Polarization-Dependent Metasurfaces Integrated with Liquid Crystals in the Visible Region", Nano Letters, 21(11): 4554–4562, (2021).

[15] Mao, C., Yang, Y., He, X., Zheng, J., Zhou, C., "Broadband reflective multi-polarization converter based on single-layer double-L-shaped metasurface", Applied Physics A, 123(12): 1–6, (2017).

[16] Li, Y., Wang, Y., Cao, Q., "A reflective multilayer polarization converter with switchable frequency band", Journal of Applied Physics, 127(4): 045301, (2020).

[17] Ako, R.T., Lee, W.S.L., Atakaramians, S., Bhaskaran, M., Sriram, S., Withayachumnankul, W., "Ultra-wideband tri-layer transmissive linear polarization converter for terahertz waves", APL Photonics, 5(4): 046101, (2020).

[18] Youn, Y., Hong, W., "Planar Dual-Band Linear to Circular Polarization Converter using Radial-Shape Multi-Layer FSS", 2018 IEEE International Symposium on Antennas and Propagation & USNC/URSI National Radio Science Meeting, Boston, MA, USA, 1465–1466, (2018).

[19] Khan, M.I., Tahir, F.A., "Simultaneous quarter-wave plate and half-mirror operation through a highly flexible single layer anisotropic metasurface", Scientific Reports, 7(1): 1–9, (2017).

[20] Xu, J., Li, R., Wang, S., Han, A.T., "Ultra-broadband linear polarization converter based on anisotropic metasurface", Optics Express, 26(20): 26235-26241, (2018).

[21] Loncar, J., Grbic, A., Hrabar, S., "A Reflective Polarization Converting Metasurface at X -Band Frequencies", IEEE Transactions on Antennas Propagation, 66(6): 3213–3218, (2018).

[22] Grady, N.K., Heyes, J.E., Chowdhury, D.R., Zeng, Y., Reiten, M.T., Azad, A.K., Taylor, A.J., Dalvit, D.A.R., Chen, H.T., "Terahertz metamaterials for linear polarization conversion and anomalous refraction", Science, 340(6138): 1304–1307, (2013).

[23] Zhang, R., You, B., Wang, S., Han, K., Han, K., Shen, X., Wang, W., Wang, W., "Broadband and switchable terahertz polarization converter based on graphene metasurfaces", Optics Express, 29(16): 24804-24815, (2021).

[24] Xu, Y., Xu, Q., Zhang, X., Feng, X., Lu, Y., Zhang, X., Kang, M., Han, J., Zhang, W., Xu, Y., Xu, Q., Zhang, X., Feng, X., Lu, Y., Han, J., Kang, M., Zhang, W., "Stereo Metasurfaces for Efficient and Broadband Terahertz Polarization Conversion", Advanced Functional Materials, 32(44): 2207269, (2022).

[25] Zou, M., Su, M., Yu, H., "Ultra-broadband and wide-angle terahertz polarization converter based on symmetrical anchor-shaped metamaterial", Optical Materials, 107: 110062, (2020).

[26] Chieh Wu, P., Sokhoyan, R., Kafaie Shirmanesh, G., Cheng, W.-H., Atwater, H.A., Wu, P.C., Sokhoyan, R., Shirmanesh, G.K., Cheng, W., Atwater Thomas J Watson, H.A., Atwater, H.A., "Near-Infrared Active Metasurface for Dynamic Polarization Conversion", Advanced Optical Materials, 9(16): 2100230, (2021).

[27] Hassanfiroozi, A., Huang, P.-S., Huang, S.-H., Lin, K.-I., Lin, Y.-T., Chien, C.-F., Shi, Y., Lee, W.-J., Wu, P.C., Hassanfiroozi, A., Huang, P.-S., Huang, S.-H., Lin, Y.-T., Chien, C.-F., Wu, P.C., Lin, K.-I., Shi, Y., Lee, W.-J., "A Toroidal-Fano-Resonant Metasurface with Optimal Cross-Polarization Efficiency and Switchable Nonlinearity in the Near-Infrared", Advanced Optical Materials, 9(21): 2101007, (2021).

[28] Nilotpal, Nama, L., Bhattacharyya, S., Chakrabarti, P., "A metasurface-based broadband quasi nondispersive cross polarization converter for far infrared region", International Journal of RF Microwave Computer-Aided Engineering, 29(10): e21889, (2019).

[29] Ding, F., Tang, S., Bozhevolnyi, S.I., "Recent Advances in Polarization-Encoded Optical Metasurfaces", Advanced Photonics Research, 2(6): 2000173, (2021).

[30] Wang, S.Y., Bi, J.D., Liu, W., Geyi, W., Gao, S., "Polarization-insensitive cross-polarization converter", IEEE Transactions on Antennas Propagation, 69(8): 4670–4680, (2021).

[31] Cui, Z., Xiao, Z., Chen, M., Lv, F., Xu, Q., "A Transmissive Linear Polarization and Circular Polarization Cross Polarization Converter Based on All-Dielectric Metasurface", Journal of Electronics Materials, 50(7): 4207–4214, (2021).

[32] Ahmad, T., Rahim, A.A., Bilal, R.M.H., Noor, A., Maab, H., Naveed, M.A., Madni, A., Ali, M.M., Saeed, M.A., "Ultrawideband Cross-Polarization Converter Using Anisotropic Reflective Metasurface", Electronics, 11(3): 487, (2022).

[33] Pouyanfar, N., Nourinia, J., Ghobadi, C., "Multiband and multifunctional polarization converter using an asymmetric metasurface", Scientific Reports, 11(1): 1–15, (2021).

[34] Guo, Y., Xu, J., Lan, C., Bi, K., "Broadband and High-efficiency Linear Polarization Converter Based on Reflective Metasurface", Engineered Science, 14(2): 39–45, (2021).

[35] Zheng, Q., Guo, C., Ding, J., "Wideband metasurface-based reflective polarization converter for linear-to-linear and linear-to-circular polarization conversion", IEEE Antennas Wireless Propagation Letters, 17(8): 1459–1463, (2018).

[36] Sun, S., Jiang, W., Gong, S., Hong, T., "Reconfigurable Linear-to-Linear Polarization Conversion Metasurface Based on PIN Diodes", IEEE Antennas Wireless Propagation Letters., 17(9): 1722–1726, (2018).

[37] Li, Z.Y., Li, S.J., Han, B.W., Huang, G.S., Guo, Z.X., Cao, X.Y., "Quad-Band Transmissive Metasurface with Linear to Dual-Circular Polarization Conversion Simultaneously", Advanced Theory and Simulations, 4(8): 2100117, (2021).

[38] Dutta, R., Ghosh, J., Yang, Z., Zhang, X., "Multi-band multi-functional metasurface-based reflective polarization converter for linear and circular polarizations", IEEE Access, 9: 152738–152748, (2021).

[39] Qiao, Q., Qiao, Q., Wang, Y., Wang, Y., Wang, Y., Yang, G., Yang, G., Yang, G., Fu, Y., Fu, Y., Liu, Y., Liu, Y., "Broadband of linear-to-linear and double-band of linear-to-circular polarization converter based on a graphene sheet with a π-shaped hollow array", Optical Materials Express, 11(9): 2952-2965, (2021).

[40] Dias, L.F.F., Jouvaud, C., Delaveaud, C., Aubert, H., "Polarization Conversion from a Two-Port Impedance Loaded Tag", In 2022 16th European Conference on Antennas and Propagation, EuCAP, 1-5, (2022).

[41] Ullah, S., Abdullah, Khan, B., Ullah, R., Ali, H., Kamal, B., "Asymmetric polarization converting metasurface for microwave applications", Optical Materials Express, 12(9): 3403-3415, (2022).

[42] Couto, M.M., Silva, M.W.B., Campos, A.L.P.S., "A novel ultra-wideband reflective cross-polarization converter based on anisotropic metasurface", Journal of Electromagnetic Waves and Applications, 35(12): 1652–1662, (2021).

[43] Mao, C., Yang, Y., He, X., Zheng, J., Zhou, C., "Broadband reflective multi-polarization converter based on single-layer double-L-shaped metasurface", Applied Physics A, 123(12): 1–6, (2017).

[44] Lin, B., Guo, J., Lv, L., Wu, J., Ma, Y., Liu, B., Wang, Z., "Ultra-wideband and high-efficiency reflective polarization converter for both linear and circular polarized waves", Applied Physics A, 125(2): 1–8, (2019).

[45] Khan, M.I., Khalid, Z., Tahir, F.A., "Linear and circular-polarization conversion in X-band using anisotropic metasurface", Scientific Reports, 9(1): 1–11, (2019).

[46] Deng, G., Yu, Z., Yin, Z., Yang, J., Li, Y., "A miniaturized and wide-angle 3D metamaterial for reflective polarization conversion", Optical Materials, 133: 113017, (2022).

[47] Nguyen, T.Q.H., Nguyen, T.K.T., Nguyen, T.Q.M., Cao, T.N., Phan, H.L., Luong, N.M., Le, D.T., Bui, X.K., Truong, C.L., Vu, D.L., "Simple design of a wideband and wide-angle reflective linear polarization converter based on crescent-shaped metamaterial for Ku-band applications", Optics Communications, 486: 126773, (2021).